

**Generalized evolutionary metadynamics for sampling the energy landscapes and its applications**Qiang Zhu,<sup>1,\*</sup> Artem R. Oganov,<sup>2,1,3</sup> Andriy O. Lyakhov,<sup>1</sup> and Xiaoxiang Yu<sup>4</sup><sup>1</sup>*Department of Geosciences, Center for Materials by Design, and Institute for Advanced Computational Science, Stony Brook University, Stony Brook, New York 11794, USA*<sup>2</sup>*Skolkovo Institute of Science and Technology, Skolkovo Innovation Center, Bldg. 3, Moscow 143026, Russia*<sup>3</sup>*Department of Problems of Physics and Energetics, Moscow Institute of Physics and Technology, 9 Institutskiy Lane, Dolgoprudny City, Moscow Region 141700, Russia*<sup>4</sup>*Department of Materials Science and Engineering, Northwestern University, Evanston, Illinois 60208, USA*

(Received 22 December 2014; revised manuscript received 27 May 2015; published 13 July 2015)

We present an automated scheme to systematically sample energy landscapes of crystalline solids, based on the ideas of metadynamics and evolutionary algorithms. Phase transitions are driven by the evolution of the order parameter (in this case, 6-dimensional order parameters composed of cell vectors components) and aided by atomic displacements corresponding to both zero and nonzero wave vectors, enabling cell size to spontaneously change during simulation. Our technique can be used for efficient prediction of stable crystal structures, and is particularly powerful for mining numerous low-energy configurations and phase transition pathways. By applying this method to boron, we find numerous energetically competitive configurations, based on various packings of B<sub>12</sub> icosahedra. We also observed a low-energy metastable structure of Si(T32) which is likely to be a product of decompression on Si-II. T32 is calculated to have a quasidirect band gap of 1.28 eV, making it promising for photovoltaic applications.

DOI: [10.1103/PhysRevB.92.024106](https://doi.org/10.1103/PhysRevB.92.024106)

PACS number(s): 61.50.Ks, 63.20.dk

**I. INTRODUCTION**

In the last decade, major advances in the field of crystal structure prediction (CSP) took place, both for organic and inorganic crystals [1,2]. Most of the advances in this field are devoted to search for the global energy minimum (most stable structure); however, attempts to explore all the low-energy metastable minima are rather limited so far. Metastable phases, although not thermodynamic equilibrium states, are very common and of great importance in materials science. For instance, carbon can exist in many distinct forms, ranging from superhard insulating diamond to ultrasoft semimetallic graphite, and many other allotropes (e.g., fullerenes, carbon nanotubes, *M*-carbon [3]), of which graphite is the only thermodynamic ground state at ordinary temperature and pressure conditions [4]. Graphite itself exists in two polytypic forms, rhombohedral and hexagonal, which only differ in the stacking sequence of the graphene layers. Rich polymorphism and polytypism are indeed common among both complex compounds and simple elements. For example, lithium at low temperatures is found to undergo a martensitic transformation from bcc to a complex close-packed rhombohedral structure (Li-9*R*) [5]. Metastable structures can be easily missed in an ordinary CSP calculation, if the search is only targeted to identify the ground state. If metastable states are of interest, attention should be paid to reconstructing the whole low-energy part of the landscape, instead of locating just the global minimum.

**II. GENERALIZED EVOLUTIONARY METADYNAMICS**

Laio and Parrinello originally proposed the metadynamics method to explore the free energy surface (FES) [6]. They

expressed the Gibbs energy as a function of a few collective variables (CVs)  $\sigma$ , by means of coarse-grained dynamics:

$$G = G^\sigma + \sum W e^{-\frac{|\sigma - \sigma(t')|^2}{2\delta\sigma^2}}. \quad (1)$$

Here, the second term is a Gaussian potential, which introduces a time-dependent bias to discourage the already sampled configuration from being visited again. With proper parametrization of the Gaussian height ( $W$ ) and width ( $\delta\sigma$ ), metadynamics efficiently reaches and crosses the transition state, thus solving an intrinsic problem of molecular dynamics (MD) simulations. This technique has been successfully applied to many problems [7]. It was found that cell shape is a good choice of CVs set for the study of solid-solid phase transitions [8]. Therefore, the total dimensionality,  $3N + 3$  for a system with  $N$  atoms, is split into 6 dimensions handled by metadynamics, and the remaining  $3N - 3$  variables explored by MD. Although it has found great success in CSP, the original version of metadynamics has challenges, in cases where MD cannot equilibrate the system at given cell shape, and where the transformation is not well described by the cell shape change (i.e., where  $3N + 3 \rightarrow 6$  reduction of dimensionality is not adequate). In principle, one can also use high-temperature MD to allow the large displacements on the atomic positions. However, the calculation will usually end up with very disordered systems.

Indeed, the  $3N - 3$  variables describing atomic positions can be transformed into a set of mutually orthonormal modes that possess valuable properties and are often used to describe transitions between crystal structures. If a structure is not dynamically stable (i.e., has phonons with imaginary frequencies), a more stable structure is obtained by following the eigenvector of the soft vibrational mode. For structures without soft modes, there is a statistically valid Bell-Evans-Polanyi principle that states that low-energy structures are usually connected by low activation barriers [9]. Low barriers are, in

\*qiang.zhu@stonybrook.edu

turn, usually related to the direction of the lowest curvature of the FES—or eigenvector of the softest vibrational mode [10].

Following this philosophy, we recently developed a hybrid technique, evolutionary metadynamics [11], where large displacements ( $d_{\max}$ ) along softest-mode eigenvectors are used to equilibrate the system (i.e., find the lowest-energy configuration) at each cell shape. The idea of using large phonon displacements was borrowed from the soft-mutation operator [12] of our evolutionary structure prediction method USPEX [13]. Furthermore, unlike the original version of metadynamics, essential elements of an evolutionary algorithm were incorporated—evolutionary metadynamics deals with a population of structures (rather than a single evolving structure) and involves a selection step, where at each cell shape the lowest-energy configuration is selected and used for making the next population of structures (each corresponding to a particular phonon displacement pattern). In Ref. [11], just like in the original metadynamics technique [7,8], only transitions between structures having the same number of atoms in the cell were allowed. The use of the dynamical matrix gives a natural recipe to overcome this limitation. To find softest modes and their eigendisplacements, we compute the dynamical matrix  $D$  at each wave vector  $\mathbf{q}$ :

$$D_{\alpha\beta}^{ij}(\mathbf{q}) = \frac{1}{(m_i m_j)^{1/2}} \sum_l \Phi_{\alpha\beta}^{ij}(0, l) \exp\{i\mathbf{q}[r_j(l) - r_i(0)]\}, \quad (2)$$

where  $m_i$  and  $m_j$  are masses of the  $i$ th and  $j$ th atoms, the sum runs over all  $l$ th unit cells, and  $\Phi_{\alpha\beta}^{ij}(0, l)$  are force constants between the atom  $i$  in the reference cell ( $l = 0$ ) and atom  $j$  in the  $l$ th cell, whose positions are described by vectors  $r_i(l)$  and  $r_j(0)$ :

$$\Phi_{\alpha\beta}^{ij}(l, l') = \frac{\partial^2 E}{\partial u_{\alpha}^i(l) \partial u_{\beta}^j(l')}, \quad (3)$$

where  $u_{\alpha}^i(l)$  denotes a displacement of an  $i$ th atom in the  $l$ th unit cell along the  $\alpha$ th coordinate axis.

Solving the secular equation with the dynamical matrix given by Eq. (2) yields both eigenvectors and frequencies of all phonon modes corresponding to the wave vector  $\mathbf{q}$ . In our original work [11] only the case  $\mathbf{q} = 0$  was studied; i.e., the system size (number of atoms in the simulation cell) was kept constant throughout the simulation, just like in normal metadynamics. By considering those nonzero  $\mathbf{q}$  vectors, it allows a simple way to consider structural modulations and complex phase transition mechanisms that involve system size variations. The extension results in the generalized evolutionary metadynamics (GEM) technique, which we present below. However, several computational problems need to be addressed.

First, the computation of the dynamical matrix (2) is very expensive at the *ab initio* level. We have simplified it [11,12,14] by taking bond hardness coefficients [15] as force constants (3). Bond hardness coefficients are computed from interatomic distances in a relaxed structure, and from the tabulated covalent radii and electronegativities of the atoms [12,15]. Then, in our dynamical matrix calculation, we have set atomic masses to unity, as here we are only interested in potential energy curvatures (which do not depend on masses) rather than frequencies (which depend on them).

Second, considering many  $\mathbf{q}$  vectors proportionally increases the number of phonon modes, and each mode corresponds to two structures (because displacements in both positive and negative directions might produce different structures). Thus, if there are  $N$  atoms in the unit cell and  $m$  wave vectors are being sampled, there will be  $6mN$  structures (e.g., for a moderate-size calculation with  $N = 30$  and  $m = 8$ , at each metastep one will have to sample 1440 structures). We found a recipe to considerably, by 1–2 orders of magnitude, reduce the number of needed phonon displacements without sacrificing the predictive power of the method. This is done through several ways. (1) Only inequivalent  $\mathbf{q}$  vectors are considered. Even for lowest-symmetry crystals this introduces a twofold saving of computational effort due to time-reversal symmetry. (2) Aufbau principle: each new added mode is chosen from a new  $\mathbf{q}$  vector, in order of increasing magnitude of the real-space modulation vector. This allows an economical sampling of all relevant wave vectors. (3) At each  $\mathbf{q}$  vector we consider only the lowest-frequency modes, typically not more than 1/3 of the total number. Among these, we exclude acoustic modes, and remove all (nearly) degenerate modes and displacement directions. With this scheme, for a system with  $N = 30$  and  $m = 8$ , it is sufficient to use 50–100 phonon displacements, and we checked that further increasing this number does not bring any practical improvements. These selected displacements typically result in distinct new structures, most of which have very low energies, indicating a remarkable efficiency of finding low-energy structures.

Comparing with original metadynamics [8], here we obtain at least one order of magnitude more low-energy structures at a similar computational cost, with the possibility of sampling cells of different sizes. At each metastep, we compare normalized energies (e.g., energies per atom) and choose the lowest-energy structure as the parent of the new generation. For this structure we compute the stress tensor at its current cell shape  $H(t)$ , and apply transformation to drive the evolution of the cell shape. Since now different structures correspond to different supercells of the original basic cell  $h(t)$ , we keep track of the supercell indices  $S(t) = [i, j, k]$  and apply deformation to the basic cell as follows:

$$h(t) = H(t) \cdot \begin{bmatrix} 1 & 1 & 1 \\ i & j & k \end{bmatrix}', \quad (4a)$$

$$h(t+1) = h(t) + \delta h |f| V^{1/3} S \otimes f \cdot h(t), \quad (4b)$$

$$H(t+1) = h(t+1) \cdot [ijk]', \quad (4c)$$

where  $S$  is the elastic compliance tensor corresponding to an elastically isotropic medium with a typical Poisson ratio 0.26, which is the border between brittle and ductile materials [16].  $\delta h$  is a stepping parameter, while the driving force  $f$  has two components according to Eq. (1): (I)  $f_{\text{real}} = V[h^{-1}(P - p)]$  is defined as the derivative of the energy with respect to  $h$ , and (II)  $f_{\text{Gaussian}}$  comes from the added Gaussian.

Finally, the scheme described above can only lead to increasingly larger supercells, which is not only computationally expensive, but also prevents many transformation paths after a supercell structure took over. To avoid this problem, every several metasteps we add an extra population generated from the original structure (after relaxation) put in the current basic

cell. In addition, for every structure we check translational symmetry and transform to a smaller cell whenever possible. This enables structural transformations with both increasing and decreasing supercell sizes.

### III. APPLICATIONS

When applied to CSP, metadynamics requires a reasonable initial configuration and then samples the phase transitions on the FES as a function of cell shape [8], while GEM does not rely only on the choice of collective variables (cell shape), but also samples the atomic displacements over different  $\mathbf{q}$  vectors. Thus it allows one to perform structure prediction by using rather simple structural types as an initial guess. For instance, we successfully identified  $\alpha$ -Ga, graphite, and diamond structures as the ground states for group III-IVA elements, by starting from a bcc structure. This differentiates our method from the original metadynamics [8]. And this success encourages us to apply GEM to more complex systems.

In our studies, the structure relaxations are done based on density functional theory (DFT) within the Perdew-Burke-Ernzerhof (PBE) generalized gradient approximation (GGA) [17] as implemented in the VASP code [18]. We used the all-electron projector-augmented wave (PAW) method and the plane wave basis set with the 600 eV kinetic energy cutoff; the Brillouin zone was sampled by uniform  $\Gamma$ -centered meshes with the reciprocal space resolution  $2\pi \times 0.06 \text{ \AA}^{-1}$ . To ensure that the obtained structures are dynamically stable, we calculated phonon frequencies throughout the Brillouin zone using the finite-displacement approach [19].

#### A. Close-packing motifs of boron

Here we first report the results on boron, an element famous for its structural complexity. The most striking feature in all the discovered boron allotropes is that boron atoms form icosahedral clusters [20,21]. Such clusters are also found in boron-rich solids [21]. The simplest structure containing icosahedron is  $\alpha$ -boron, which is based on a distorted cubic packing of icosahedra. The resulting crystal structure has rhombohedral symmetry (space group  $R\bar{3}m$ ). All  $B_{12}$  units in the structure follow the ‘‘ABC’’ stacking sequence along the [0001] direction. It is well known that ABC stacking (or fcc) has four equivalent close-packed planes. One may wonder about the possibility of other close-packed arrangement of the  $B_{12}$  icosahedra.

Using the GEM technique, we performed a simulation starting from a 12-atom primitive cell of  $\alpha$ -boron phase. Figure 1(a) shows the evolution of the enthalpy.  $\alpha$ -B persists until the 25th generation. Then upon sufficient cell deformation and aided by low-energy modes, it undergoes a transition to a  $Cmca$  phase. The structure has been proposed by Pickard [22] and discussed by He [23], who, however, both failed to notice that this is a closed-packed polytype of  $\alpha$ -B. As we mentioned, an important feature of (G)EM is that the sampling space at each metastep is much more global than traditional MD, and typically yields many structures. By a close examination of the results, we found a series of low-energy configurations (see Table I). Clearly, all the low-energy

TABLE I. Crystallographic data of various boron allotropes at zero pressure.

$2O, Cmca, a = 4.884 \text{ \AA}, b = 8.851 \text{ \AA}, c = 8.065 \text{ \AA}$				
Atomic coordinates				
B	8f	0.0000	0.2361	0.5683
B	8f	0.0000	0.4373	0.5756
B	8g	0.6817	0.0051	0.2500
B	8g	0.3229	0.3327	0.2500
B	16h	0.7032	0.3313	0.6391
$4O, Cmca, a = 4.892 \text{ \AA}, b = 8.841 \text{ \AA}, c = 16.098 \text{ \AA}$				
Atomic coordinates				
B	8f	0.0000	0.3909	0.9143
B	8f	0.0000	0.0625	0.6591
B	8f	0.0000	0.5928	0.5927
B	8f	0.5000	0.7646	0.6621
B	8g	0.8235	0.9939	0.7500
B	8g	0.6812	0.8218	0.7500
B	16h	0.8214	0.6642	0.5030
B	16h	0.2040	0.0024	0.4446
B	16h	0.7961	0.6580	0.8054
$9M, C2/m, a = 8.846 \text{ \AA}, b = 4.891 \text{ \AA}, c = 12.459 \text{ \AA}, \beta = 104.2^\circ$				
Atomic coordinates				
B	4i	0.2796	0.0000	0.0451
B	4i	0.0697	0.0000	0.3859
B	4i	0.1608	0.0000	0.2842
B	4i	0.3637	0.0000	0.2876
B	4i	0.8646	0.0000	0.3764
B	4i	0.4198	0.5000	0.9495
B	8j	0.9371	0.1814	0.8329
B	8j	0.2992	0.2035	0.9074
B	8j	0.3906	0.1768	0.1665
B	8j	0.7521	0.2037	0.2404
B	8j	0.8344	0.1786	0.4959
B	8j	0.9769	0.2961	0.4262
$P3_21, a = 5.041 \text{ \AA}, c = 12.031 \text{ \AA}$				
Atomic coordinates				
B	6c	0.3259	0.1062	0.1095
B	6c	0.9858	0.4827	0.4102
B	6c	0.6678	0.4401	0.3256
B	6c	0.8059	0.6909	0.2071
B	6c	0.2063	0.8752	0.9922
B	6c	0.9291	0.9232	0.0712
$P2_1/c, a = 4.354 \text{ \AA}, b = 4.965 \text{ \AA}, c = 8.734 \text{ \AA}, \beta = 119.1^\circ$				
Atomic coordinates				
B	4e	0.3247	0.6714	0.6139
B	4e	0.1836	0.8377	0.3949
B	4e	0.3755	0.1649	0.4619
B	4e	0.5541	0.3368	0.6835
B	4e	0.2485	0.3327	0.2573
B	4e	0.1058	0.3329	0.5408

structures in Fig. 1 are based on the packing of  $B_{12}$  icosahedra. More interestingly, we find the most energetically competitive structures have various close packings (ABC, AB, ABAC, ABABCBCAC), as shown in Figs. 1(c)–1(f). Those include two different structures with space group  $Cmca$  with AB and ABAC stackings, another  $C2/m$  structure with ABABCBCAC stacking. However, polytypism involves shifting of  $(1\bar{1}\bar{1})$  layers in  $\alpha$ -boron, rather than (0001). Therefore, we name

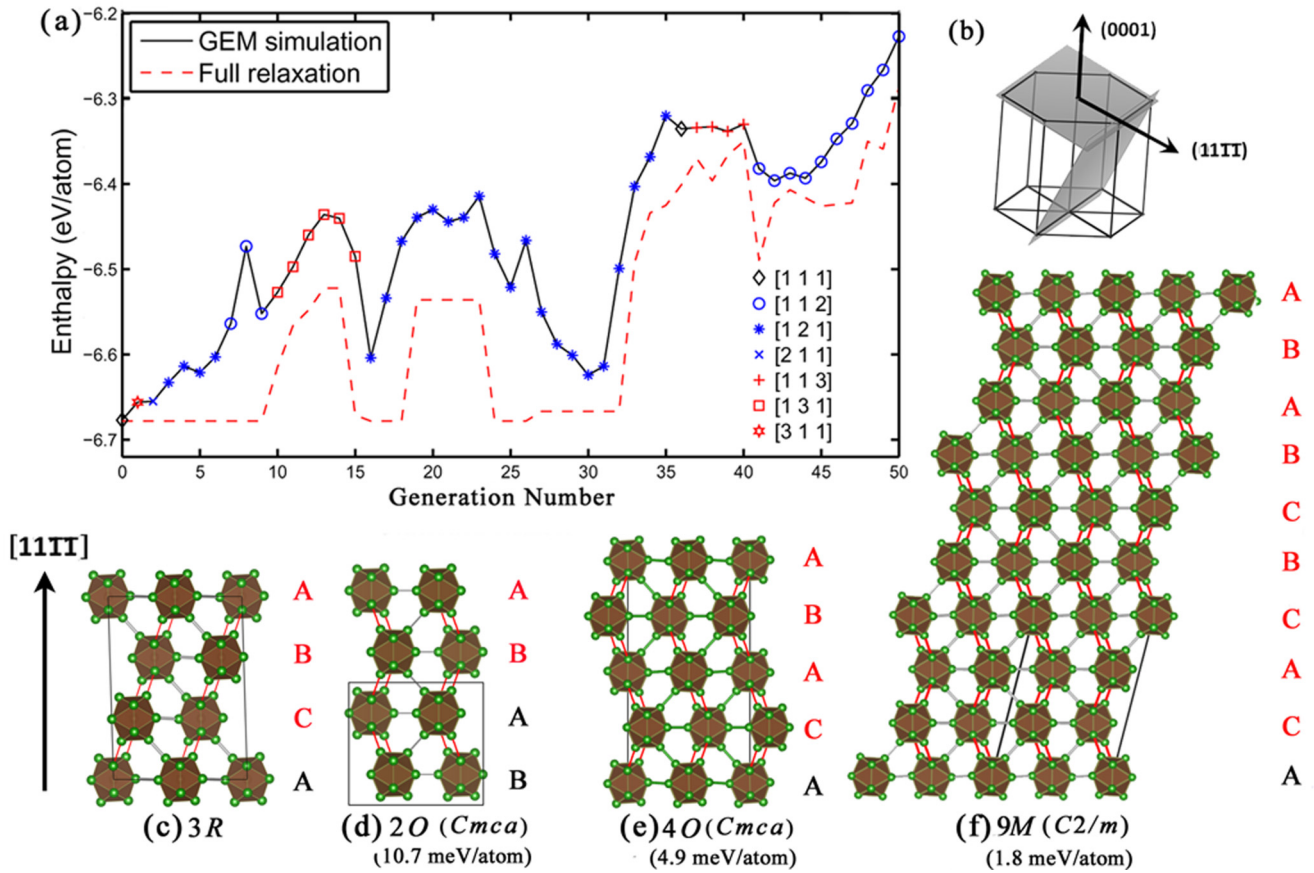


FIG. 1. (Color online) (a) GEM simulations starting from the primitive cell of  $\alpha$ -B (the supercell size of each structure is indicated by different marker symbols); (b) illustration of two close-packed planes (0001) and (11 $\bar{1}$ ) in  $\alpha$ -B based on hexagonal lattice setting; low-energy configurations are identified as a pseudo-close-packing behavior in different stacking sequences of (c) ABC ( $\alpha$ -B), (d) AB (space group  $Cmca$ ), (e) ABAC (space group  $Cmca$ ), (f) ABABCBCAC (space group  $C2/m$ ).

the new structures as  $2O$  for AB stacking,  $4O$  for ABAC stacking, and  $9M$  for ABABCBCAC stacking. For the same reason,  $\alpha$ -boron can be denoted as  $3R$ . Obviously, there can be an infinite series of energetically close polytypes constructed in this way.

In addition to those structures of boron shown in Fig. 1, we found that many low-energy structures are not closed-packed, but still based on the packing of  $B_{12}$  icosahedra, and one representative ( $P3_221$ ) is shown in Fig. 2(a). This structure has

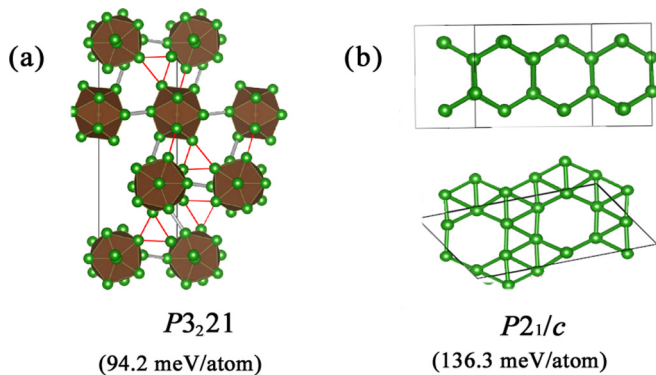


FIG. 2. (Color online) Additional representative low-energy structures (a)  $P3_221$  structure, (b)  $P2_1/c$  structure.

higher energy (94.2 meV/atom relative to  $\alpha$ -B) than the close-packed counterparts. The other one, the  $P2_1/c$  structure (Fig. 2) represents another group of structures which do not contain  $B_{12}$  units, and it has much higher energy (136.3 meV/atom) than that of  $\alpha$ -B. We note that the structure shares similarity with the planar  $\alpha$ -sheet structure that has been widely investigated by theoretical calculations [24].

All the presented structures are dynamically stable [25], indicating that these allotropes can exist long at ambient conditions. Transitions between close-packing structures have been observed and extensively studied for metals and are known to have low activation barriers—however, covalent bonding in boron will make the barriers very high. Twinning and stacking faults commonly observed in chemical vapor deposited films are due to the random occurrence of hexagonal stacking in a cubic stacking sequence [26]. It remains to be seen whether the newly predicted boron stackings can be produced in this way. One can also expect the formation of these new stackings at twin boundaries in  $\alpha$ -boron.

### B. Decompression on Si-II

Silicon is another element which has been intensely investigated. It is well known that silicon exhibits very rich polymorphism under pressure. Upon increase of pressure, silicon undergoes a series of phase transitions: I (cubic

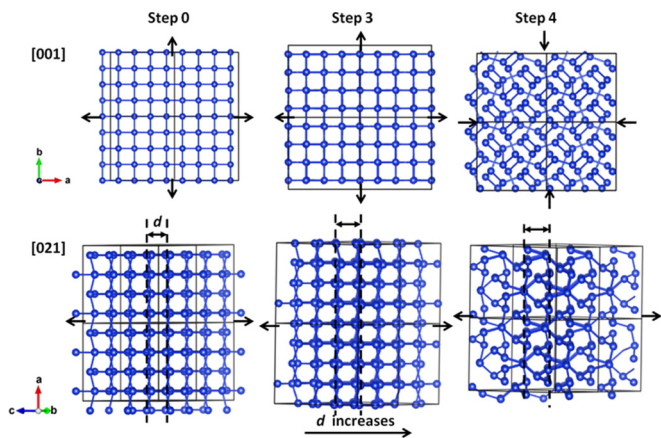


FIG. 3. (Color online) The first stage of phase transition observed in GEM simulation. The arrows on the cells represent the direction of stress on each  $a, b, c$  vector.  $d$  is the interlayer distance perpendicular to the (201) planes.

diamond)  $\rightarrow$  II ( $\beta$ -Sn)  $\rightarrow$  XI ( $Imma$ )  $\rightarrow$  V (simple hexagonal)  $\rightarrow$  VI ( $Cmca$ )  $\rightarrow$  VII (hcp)  $\rightarrow$  X (fcc). A recent metadynamics simulation by employing a high dimensional neural network potential has successfully reproduced this sequence [27]. However, the above transitions are not fully reversible upon decompression [28,29]. The Si-II phase transforms to an exotic semimetallic phase R8 (Si-XII) at 9.3 GPa, and further to another metastable cubic form BC8 (Si-III) that persists until ambient conditions. The transition mechanism upon decompression has not been fully understood. It has been also found that both BC8 and R8 can coexist in the indentations produced by a nanoindenter on a single-crystalline silicon wafer as a result of the residual compressive stresses [30]. Such irreversibility indicates a chance to synthesize new metastable forms by high-pressure modification. The quest for new forms of silicon surges because of photovoltaic application [31–33]. In order to achieve a better absorption in the visible light, the ideal material should have a direct band gap of 1–1.5 eV, and strong absorption within the solar spectrum.

Several GEM simulations at different pressure conditions were performed by starting from the Si-II structure which has been fully relaxed at 10 GPa. By varying the Gaussian parameters and  $d_{max}$ , we observed different products such as cubic diamond, hexagonal diamond, and many other metastable structures based on the modification of diamond which have been made by other groups [33,34].

However, we are interested in those forms which have been observed in experiments. Therefore, we intentionally decreased  $d_{max}$  and started from a  $2 \times 2 \times 1$  supercell, in which we were able to obtain the transition path from Si-II to Si-III (BC8). We reran this calculation by using a larger population size (120 for a 64-atom system). The phase transitions can be understood via two stages as follows.

At the beginning, Si-II undergoes lattice expansion nearly uniformly, as the initial configuration is relaxed at 10 GPa. After a few generations, the expansions in the  $a, b$  directions were compensated by Gaussian force, while the lattice still increases along the  $c$  direction. As shown in Fig. 3, the (021) stacking layers are deformed and undergo a reconstruction due

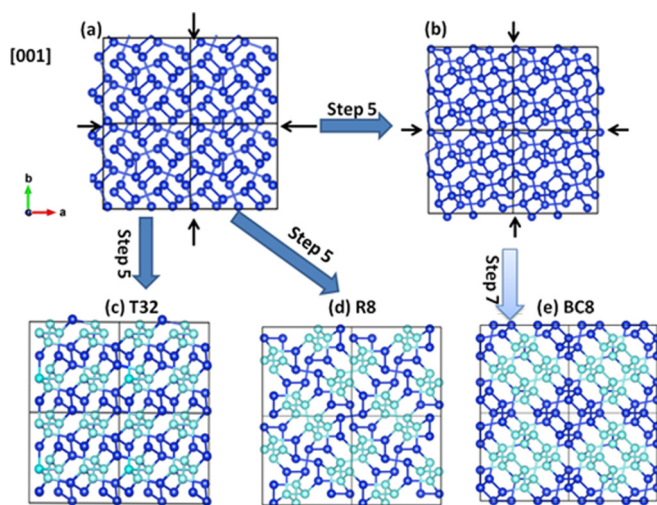


FIG. 4. (Color online) The second stage of phase transition observed in GEM simulation. The arrows on the cells represent the stresses on each  $a, b$  direction. (a) and (b) represent two intermediate structures shown in the simulation; (c)  $2 \times 2 \times 1$  supercell of R8 structure; (d)  $2 \times 2 \times 1$  supercell of BC8 structure; (e)  $2 \times 2 \times 1$  supercell of T32 structure [space group  $P4_21c$ ,  $a = 9.416 \text{ \AA}$ ,  $c = 6.639 \text{ \AA}$ , Si1(0.479, 0.375, 0.231), Si2(0.124, 0.523, 0.221), Si3(0.229, 0.620, 0.521), Si4(0.372, 0.728, 0.976)]. The tetragonal spiral chains are highlighted in cyan.

to this uneven strain distribution, which leads to the occurrence of spiral chains at step 4.

We found that further deformation at the next step can easily lead to reconstructions in many ways, by using different vibrational modes. As shown in Fig. 4, we observed that the softmutated structures can be characterized by the arrangements of the tetragonal spiral chains. After full relaxation of (c) and (d), we successfully obtained R8 and another phase in tetragonal form. Although the best survival in this generation is not dynamically stable, we found the BC8 structure as the best survival in the later generation [from (b) to

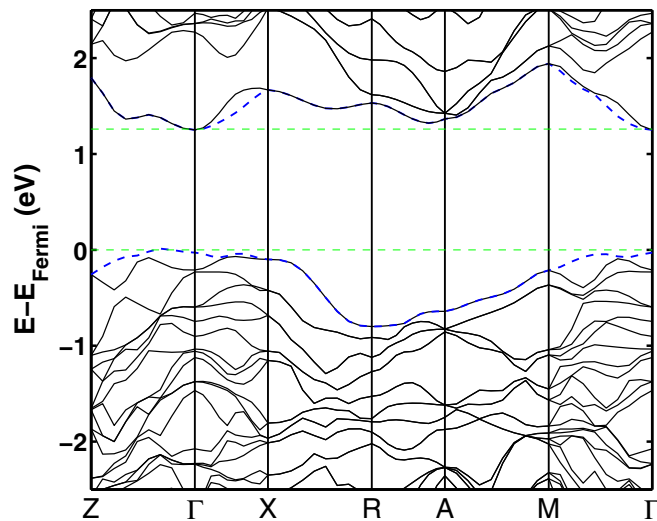


FIG. 5. (Color online) The HSE06 band structure of Si-T32 structure.

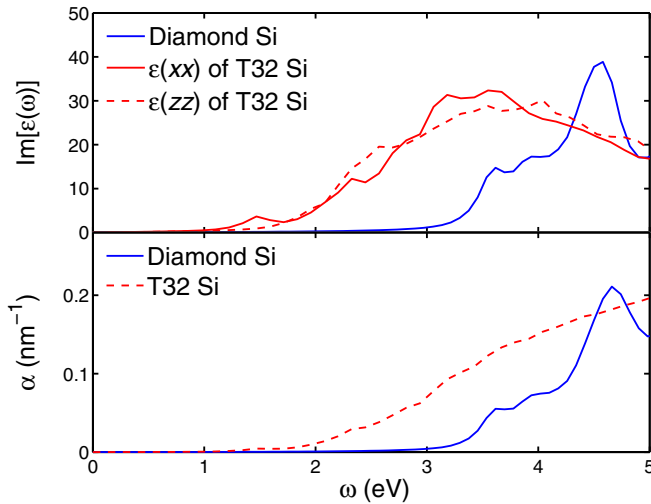


FIG. 6. (Color online) The calculated imaginary part of dielectric functions and optical absorption coefficient for Si-T32. The results for Si diamond phase are also shown for comparison.

(e) in Fig. 4]. Interestingly, all structures (T32, R8, and BC8) can be characterized by different arrangements of tetragonal spiral chains.

All three structures have very close energetics, which are 160 meV/atom (BC8), 161 meV/atom (R8), and 164 meV/atom (T32) higher than Si-I at ambient pressure. Although closely associated in both topology and energetics, they exhibit different electronic properties. Both BC8 and R8 are semimetallic [35], while T32 is calculated to be a semiconductor within the PBE functional. Standard DFT is well known to underestimate the band gaps, while the HSE06 functional is considered to be very accurate for silicon [32,33,36]. As shown in Fig. 5, the valence band maximum (VBM) is located at  $(0, 0, 1/6)$ , but is only 0.03 eV higher than the  $\Gamma$  point. The conduction band minimum (CBM) is right at the  $\Gamma$  point, thus making T32 a semiconductor with a quasidirect band gap of 1.28 eV at the  $\Gamma$  point. The imaginary part of the dielectric function for T32 within the HSE06 functional is also shown in Fig. 6. Compared with Si-I, the optical absorption in T32 starts from a much lower energy ( $\sim 1.28$  eV), which makes T32 very attractive for solar cell applications.

Different from the previously proposed Si allotropes [32–34], T32 shares many similarities with BC8 and R8. Thus it is very likely to be synthesized from Si-II as well, by using the same experimental protocols such as diamond anvil cell [28], nanoindentation [30], and perhaps elastic strain engineering [37]. We provide the comparison of simulated x-ray diffraction pattern for the BC8, R8, and T32 structures as shown in Fig. 7. Although all three structures share the same peaks with

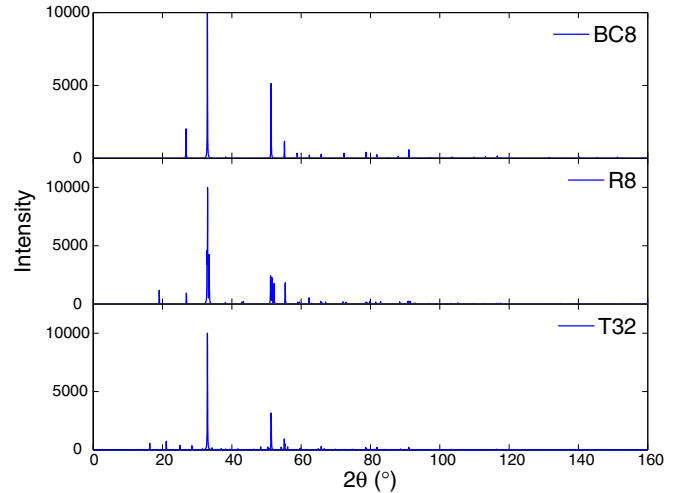


FIG. 7. (Color online) Comparison of simulated x-ray diffraction patterns for (a) BC8, (b) R8, and (c) T32 under ambient conditions, respectively. The patterns were simulated using mercury with an x-ray wavelength of 1.54056 Å.

strongest intensity, the diffraction patterns are clearly different from each other, especially at the low-angle region, which can be used to distinguish them in future experiments.

#### IV. CONCLUSIONS

In summary, we have developed and used a specially designed GEM technique to explore energy landscapes. This method allows us to identify a number of low-energy configurations through complex transition mechanisms, accessible even when starting from a rather simple structure. We illustrated the power by applying it to study elemental boron and silicon. The predicted allotropes of these elements are energetically competitive and topologically related to some known phases, thus likely to be synthesized by experiments. The GEM technique can be generally used to systematically search for metastable structures in other systems.

#### ACKNOWLEDGMENTS

Calculations were performed at the supercomputer of the Center for Functional Nanomaterials, Brookhaven National Laboratory, which is supported by the U.S. Department of Energy, Office of Basic Energy Sciences, under Contract No. DE-AC02-98CH10086. We thank the DARPA (Grant No. W31P4Q1210008), the Government (No. 14.A12.31.0003) of the Russian Federation, Foreign Talents Introduction and Academic Exchange Program (No. B08040), and SUNY 4E Networks of Excellence for financial support.

- [1] D. A. Bardwell *et al.*, *Acta Cryst.* **B67**, 535 (2011).
- [2] A. R. Oganov, editor, *Modern Methods of Crystal Structure Prediction* (Wiley-VCH, Weinheim, 2010).
- [3] S. E. Boulfelfel, A. R. Oganov, and S. Leoni, *Sci. Rep.* **2**, 471 (2012).
- [4] A. Hirsch, *Nat. Mater.* **9**, 868 (2010).

- [5] A. C. Redfield and A. M. Zangwill, *Phys. Rev. B* **34**, 1378 (1986).
- [6] A. Laio and M. Parrinello, *Proc. Natl. Acad. Sci. USA* **99**, 12562 (2002).
- [7] A. Barducci, M. Bonomi, and M. Parrinello, *Wiley Interdisciplinary Reviews: Comput. Mol. Sci.* **1**, 826 (2011).

- [8] R. Martoňák, A. Laio, and M. Parrinello, *Phys. Rev. Lett.* **90**, 075503 (2003).
- [9] F. Jensen, *Computational Chemistry* (Wiley, New York, 1999).
- [10] S. Goedecker, *J. Chem. Phys.* **120**, 9911 (2004).
- [11] Q. Zhu, A. R. Oganov, and A. O. Lyakhov, *CrystEngComm* **14**, 3596 (2012).
- [12] A. O. Lyakhov, A. R. Oganov, and M. Valle, *Comput. Phys. Commun.* **181**, 1623 (2010).
- [13] A. R. Oganov and C. W. Glass, *J. Chem. Phys.* **124**, 244704 (2006).
- [14] A. O. Lyakhov, A. R. Oganov, H. T. Stokes, and Q. Zhu, *Comput. Phys. Commun.* **184**, 1172 (2013).
- [15] K. Li, X. Wang, F. Zhang, and D. Xue, *Phys. Rev. Lett.* **100**, 235504 (2008).
- [16] S. F. Pugh, *Philos. Mag.* **45**, 823 (1954).
- [17] J. P. Perdew, K. Burke, and M. Ernzerhof, *Phys. Rev. Lett.* **77**, 3865 (1996).
- [18] G. Kresse and J. Furthmuller, *Phys. Rev. B* **54**, 11169 (1996).
- [19] A. Togo, F. Oba, and I. Tanaka, *Phys. Rev. B* **78**, 134106 (2008).
- [20] A. R. Oganov, J. Chen, C. Gatti, Y. Ma, Y. Ma, C. W. Glass, Z. Liu, T. Yu, O. O. Kurakevych, and V. L. Solozhenko, *Nature (London)* **457**, 863 (2009).
- [21] B. Albert and H. Hillebrecht, *Angew. Chem. Int. Ed.* **48**, 8640 (2009).
- [22] C. J. Pickard and R. J. Needs, *J. Phys.: Condens. Matter* **23**, 053201 (2011).
- [23] C. He and J. X. Zhong, *AIP Adv.* **3**, 042138 (2013).
- [24] H. Tang and S. Ismail-Beigi, *Phys. Rev. Lett.* **99**, 115501 (2007).
- [25] See Supplemental Material at <http://link.aps.org/supplemental/10.1103/PhysRevB.92.024106> for dynamical stability of various boron and silicon allotropes.
- [26] Y. Lifshitz, X. Duan, N. Shang, Q. Li, L. Wan, I. Bello, and S. Lee, *Nature (London)* **412**, 404 (2001).
- [27] J. Behler, R. Martoňák, D. Donadio, and M. Parrinello, *Phys. Rev. Lett.* **100**, 185501 (2008).
- [28] J. Crain, G. J. Ackland, J. R. Maclean, R. O. Piltz, P. D. Hatton, and G. S. Pawley, *Phys. Rev. B* **50**, 13043 (1994).
- [29] Y.-X. Zhao, F. Buehler, J. R. Sites, and I. L. Spain, *Solid State Commun.* **59**, 679 (1986).
- [30] Z. Zeng, Q. Zeng, W. L. Mao, and S. Qu, *J. Appl. Phys.* **115**, 103514 (2014).
- [31] D. Y. Kim, S. Stefanoski, O. O. Kurakevych, and T. A. Strobel, *Nat. Mater.* **14**, 169 (2015).
- [32] H. J. Xiang, B. Huang, E. Kan, S.-H. Wei, and X. G. Gong, *Phys. Rev. Lett.* **110**, 118702 (2013).
- [33] Q. Wang, B. Xu, J. Sun, H. Liu, Z. Zhao, D. Yu, C. Fan, and J. He, *J. Am. Chem. Soc.* **136**, 9826 (2014).
- [34] S. Botti, J. A. Flores-Livas, M. Amsler, S. Goedecker, and M. A. L. Marques, *Phys. Rev. B* **86**, 121204 (2012).
- [35] B. G. Pfrommer, M. Côté, S. G. Louie, and M. L. Cohen, *Phys. Rev. B* **56**, 6662 (1997).
- [36] A. V. Krukau, O. A. Vydrov, A. F. Izmaylov, and G. E. Scuseria, *J. Chem. Phys.* **125**, 224106 (2006).
- [37] J. Li, Z. Shan, and E. Ma, *MRS Bull.* **39**, 108 (2014).